Relationship Between Macular Curvature and Common Causative Genes of Retinitis Pigmentosa in Japanese Patients

Yoshito Koyanagi,[1–4] Shinji Ueno,[1] Yasuki Ito,[1] Taro Kominami,[1] Shiori Komori,[1] Masato Akiyama,[2–5] Yusuke Murakami,[2] Yasuhiro Ikeda,[2,6] Koh-Hei Sonoda,[2] and Hiroko Terasaki[1]

[1]Department of Ophthalmology, Nagoya University Graduate School of Medicine, Nagoya, Japan
[2]Department of Ophthalmology, Graduate School of Medical Sciences, Kyushu University, Fukuoka, Japan
[3]Laboratory for Statistical Analysis, RIKEN Center for Integrative Medical Sciences, Kanagawa, Japan
[4]Laboratory for Statistical and Translational Genetics, RIKEN Center for Integrative Medical Sciences, Kanagawa, Japan
[5]Department of Ocular Pathology and Imaging Science, Graduate School of Medical Sciences, Kyushu University, Fukuoka, Japan
[6]Department of Ophthalmology, Faculty of Medicine, University of Miyazaki, Miyazaki, Japan

Correspondence: Shinji Ueno, Department of Ophthalmology, Nagoya University Graduate School of Medicine, 65 Tsurumai-cho, Showa-ku, Nagoya 466-8550, Japan; ueno@med.nagoya-u.ac.jp.

Received: February 28, 2020
Accepted: June 18, 2020
Published: August 4, 2020

Citation: Koyanagi Y, Ueno S, Ito Y, et al. Relationship between macular curvature and common causative genes of retinitis pigmentosa in Japanese patients. *Invest Ophthalmol Vis Sci.* 2020;61(10):6. https://doi.org/10.1167/iovs.61.10.6

Purpose. To determine the relationship between the macular curvature and the causative genes of retinitis pigmentosa (RP).

Methods. We examined the medical records of the right eyes of 65 cases with RP (31 men and 34 women; average age, 47.6 years). There were 31 cases with the *EYS* variants, 11 cases with the *USH2A* variants, six cases with the *RPGR* variants, 13 cases with the *RP1* variants, and four cases with the *RP1L1* variants. The mean curvature of Bruch's membrane was calculated within 6 mm of the fovea as the mean macular curvature index (MMCI, 1/µm). We used multiple linear regression analysis to determine the independence of the causative genes contributing to the MMCIs after adjustments for age, sex, axial length, and width of the ellipsoid zone.

Results. The median MMCI was -31.2×10^{-5}/µm for the *RPGR* eyes, -16.5×10^{-5}/µm for the *RP1L1* eyes, -13.0×10^{-5}/µm for the *RP1* eyes, -9.8×10^{-5}/µm for the *EYS* eyes, and -9.0×10^{-5}/µm for the *USH2A* eyes. Compared with the *EYS* gene as the reference gene, the *RPGR* gene was significantly related to the MMCI values after adjusting for the other parameters ($P = 5.30 \times 10^{-6}$). In contrast, the effects of the other genes, *USH2A*, *RP1,* and *RP1L1*, were not significantly different from that of the *EYS* gene ($P = 0.26$, $P = 0.49$, and $P = 0.92$, respectively).

Conclusions. The *RPGR* gene had a stronger effect on the steep macular curvature than the other ciliopathy-related genes.

Keywords: macular curvature, causative genes, retinitis pigmentosa, spectral-domain optical coherence tomography, mean macular curvature index

Retinitis pigmentosa (RP) is the most common hereditary retinal degenerative disease worldwide.[1] It is characterized by a reduction in vision, visual field constriction, and night blindness, which develop due to the dysfunction and death of the rod photoreceptors. These changes lead to the death of the cone cells and a reduction of the visual acuity.[2,3]

To date, 89 genes causing nonsyndromic RP have been registered in the Retinal Information Network (https://sph.uth.edu/retnet/. Accessed on November 28, 2019). The recent adaptation of high-throughput DNA sequencing technologies has accelerated the identification of the causative genes of Japanese patients with RP, and these studies have revealed the major causative genes in this population.[4–6] Some of these major genes were categorized into the ciliopathy-related genes (e.g., the *USH2A*, *RPGR*, *RP1,* and *RP1L1* genes),[7–12] and it was also suggested that the function of the *EYS* protein is associated with the cilia.[1,13,14]

Recently, several studies have reported that steep macular curvatures were observed in the eyes of patients with various inherited retinal disorders, including retinal ciliopathy, Joubert syndrome, Leber's congenital amaurosis, and RP without high myopia.[15–20] In our earlier study, we established that the mean macular curvature index (MMCI) can be an additional parameter of the ocular anatomy that can be used to quantify the degree of macular curvature. The MMCI was determined from the spectral-domain optical coherence tomography (SD-OCT) images. We showed that the macular curvature of eyes with RP was steeper than that of normal eyes.[21] We also found a significant relationship between the age, axial length (AL), and the width of the ellipsoid zone

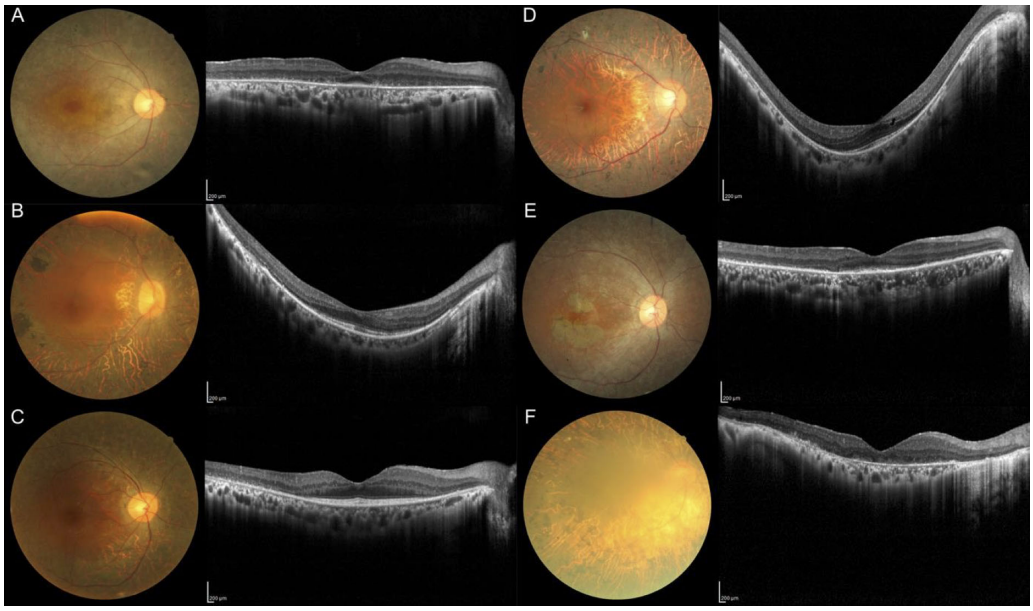

Figure 1. Fundus photographs and SD-OCT images of representative cases with RP for each causative gene. A: **Case 1** is a 50-year-old female that was a case with *EYS*-related retinitis pigmentosa (RP) with an ellipsoid zone (EZ) of 635 µm. The mean macular curvature index (MMCI) was -0.3×10^{-5} µm^{-1}. The axial length (AL) was 24.81 mm. B: **Case 2** is a 48-year-old female with *EYS*-related RP with an EZ of 2762 µm. Bruch's membrane has a steeper curvature than that of Case 1. The MMCI was -36.0×10^{-5} µm^{-1}. The AL was 24.52 mm. C: **Case 3** is a 53-year-old male with *USH2A*-related RP and an EZ of 3266 µm. The MMCI was -8.0×10^{-5} µm^{-1}. The AL was 23.81 mm. D: **Case 4** is a 34-year-old male who is a case of *RPGR*-related RP with an EZ of 2333 µm. The OCT image shows a steep macular curvature. The MMCI was -47.8×10^{-5} µm^{-1}. The AL was 25.83 mm. E: **Case 5** is a 23-year-old female who is a case of *RP1*-related RP without an intact EZ (0 µm). This case had a relatively flat macular line. The MMCI was -5.62×10^{-5} µm^{-1}. The AL was 21.81 mm. F: **Case 6** is a 67-year-old male who is a case of *RP1L1*-related RP without an intact EZ (0 µm). The MMCI was -18.01×10^{-5} µm^{-1}. The AL was 24.09 mm.

(EZ) and the steepness of the macular curvature in the RP cases.[21]

Considering the genetic and clinical heterogeneity of RP, comparisons of the MMCIs associated with the causative genes is important for further understanding of the pathology of RP.[22]

Therefore, the aim of this study was to assess the relationship between the macular curvature and the causative genes for RP.

Methods

Subjects

We reviewed the medical records of the right eye of 72 cases with typical RP from two facilities, Nagoya University Hospital (n = 37) and Kyushu University Hospital (n = 35), which were examined between 2002 and 2019. These cases had been genetically diagnosed with the five most frequent causative genes of RP (*EYS*, *USH2A*, *RPGR*, *RP1,* and *RP1L1*) in the Japanese population.[6] The clinical diagnosis was based on the history of night blindness, ring scotoma and/or constriction of the visual fields, and severe rod-cone dysfunction or nonrecordable electroretinograms. In addition, an attenuation of the retinal vessels and bone spicule-like pigment clumping in the mid-peripheral and peripheral retina were detected by experienced ophthalmologists. We excluded seven cases (four *EYS* eyes, one *USH2A* eye, one *RPGR* eye, and one *PR1* eye) due to incomplete clinical data, such as the visual acuity (n = 2), AL (n = 1), and SD-OCT images (n = 4). In the end, we studied 65 cases.

This retrospective study was approved by the ethics committee of each hospital (Nagoya University 16-0538-3, Kyushu University 2019-136) and was conducted in accordance with the tenets of the Declaration of Helsinki on biomedical research involving human subjects. The institutional review boards also waived the need for a written informed consent from each patient because the study design was a retrospective chart examination.

Measurements of Ocular Parameters

The best-corrected visual acuity (BCVA) was measured on the same day as the SD-OCT images were taken. For the statistical analyses, we converted the decimal value to logMAR units. We used an IOLMaster (Carl Zeiss Meditec, Dublin, CA, USA) to measure the AL of the eyes.

We selected the horizontal scanned OCT images consisting of 100 averaged images with the eye-tracking system functioning for the analyses. To adjust the size of each image, we corrected for the differences in the pixel resolution between the longitudinal and transverse directions. We measured the width of the EZ between the borders where the EZ band touched the upper surface of the retinal pigment epithelium with the built-in calipers using the Heidelberg Eye Explorer software (Heidelberg Engineering, Heidelberg, Germany). If the entire length of the EZ line exceeded the size of the OCT image, the borders of the EZ line were set to be that of the OCT image.[23]

Measurement of Macular Curvature

We calculated the MMCI as an objective index of the macular curvature as described in detail.[21] Briefly, we quantitatively analyzed the reflective line corresponding to Bruch's membrane across the fovea (yellow line in Fig. 1A in Komori

Investigative Ophthalmology & Visual Science

Table 1. Genetic Diagnosis of Patients With RP

ID	Age, y	Gender	Causative Genes	Genetic Inheritance Form	Variant 1	Zygosity 1	Variant 2	Zygosity 2
N-27	27	F	*EYS*	AR	p.(Ser1653fs)	Homo	—	—
N-38	54	M	*EYS*	AR	p.(Ser1653fs)	Hetero	p.(Tyr2935*)	Hetero
N-122	49	M	*RPGR*	XL	p.(G1u746fs)	Hemi	—	—
N-71	44	F	*EYS*	AR	p.(Ser1653fs)	Homo	—	—
N-109	59	M	*USH2A*	AR	p.(Ser4748Phe)	Hetero	p.(Cys934Trp)	Hetero
N-167	34	F	*EYS*	AR	p.(Ser1653fs)	Homo	—	—
N-168	29	M	*USH2A*	AR	p.(Thr3667Pro)	Hetero	p.(Val164Phe)	Hetero
N-169	51	F	*EYS*	AR	p.(AIa2736Pro)	Hetero	p.(GIn203*)	Hetero
N-180	61	F	*EYS*	AR	p.(Ser1653fs)	Hetero	p.(Gly2186G1u)	Hetero
N-183	70	F	*EYS*	AR	p.(Tyr2935*)	Hetero	p.(Asn404fs)	Hetero
N-208	48	F	*USH2A*	AR	p.(Ser5060Pro)	Hetero	p.(Ser4748Phe)	Hetero
N-224	39	M	*EYS*	AR	p.(Tyr2555fs)	Hetero	p.(Cys211Tyr)	Hetero
N-225	37	M	*RPGR*	XL	p.(G1u746fs)	Hemi	—	—
N-250	71	M	*RP1*	AD	p.(G1u661*)	Hetero	—	—
N-257	48	F	*EYS*	AR	p.(Ser1653fs)	Hetero	p.(AIa2498Pro)	Hetero
N-259	46	F	*EYS*	AR	p.(Gly2186G1u)	Homo	—	—
N-303	60	F	*EYS*	AR	p.(Asp498fs)	Hetero	p.(Cys211Tyr)	Hetero
N-37	57	F	*EYS*	AR	p.(Gly2799fs)	Hetero	p.(Arg1870Trp)	Hetero
N-39	31	F	*RP1*	AR	p.(Tyr1352Alafs*9)	Homo	—	—
NA0048	19	F	*RP1*	AR	p.(Tyr1352Alafs*9)	Homo	—	—
NA0070	38	F	*RP1*	AR	p.(Tyr1352Alafs*9)	Homo	—	—
N-34	47	M	*EYS*	AR	p.(Tyr2935*)	Hetero	p.(Gly2186G1u)	Hetero
N-75	64	F	*USH2A*	AR	p.(Cys934Trp)	Hetero	p.(G1n4371fs)	Hetero
NA0209	19	M	*RP1*	AR	p.(Tyr1352Alafs*9)	Hetero	p.(Cys1399Leufs*5)	Hetero
N-228	77	F	*EYS*	AR	p.(Gy2186G1u)	Hetero	p.(Tyr2935*)	Hetero
N-233	47	M	*RPGR*	XL	p.(G1u802fs)	Hemi	—	—
N-294	43	M	*USH2A*	AR	p.(Cys934Trp)	Homo	—	—
N-298	22	M	*RPGR*	XL	p.(Thr575fs)	Hemi	—	—
NA1048	23	M	*RP1*	AR	p.(Tyr1352Alafs*9)	Homo	—	—
N-1201	36	F	*RP1*	AR	p.(Tyr1352Alafs*9)	Hetero	p.(Cys1399Leufs*5)	Hetero
NAl209	29	F	*RP1*	AR	p.(Tyr1352Alafs*9)	Hetero	p.(Cys1399Leufs*5)	Hetero
OPH-783	35	M	*RPGR*	XL	p.?	Hemi	—	—
OPH-209	49	M	*EYS*	AR	p.(Ser1653fs)	Hetero	p.(Trp2640*)	Hetero
OPH-499	64	F	*EYS*	AR	p.(Ser1653fs)	Homo	—	—
OPH-39	69	M	*RPGR*	XL	p.(Gly718fs)	Hemi	—	—
OPH-753	48	F	*USH2A*	AR	p.(Cys934Trp)	Hetero	p.(G1u1985Lys)	Hetero
OPH-423	48	F	*EYS*	AR	p.(Ser1653fs)	Homo	—	—
OPH-985	42	M	*EYS*	AR	p.(Tyr2935*)	Hetero	p.(Gly2186G1u)	Hetero
OPH-616	43	M	*EYS*	AR	p.(Ser1653fs)	Homo	—	—
OPH-183	68	F	*RP1L1*	AR	p.(Arg658*)	Hetero	p.(G1u501*)	Hetero
OPH-302	54	M	*USH2A*	AR	p.(Arg1870Trp)	Hetero	p.(Gly2752Arg)	Hetero
OPH-570	54	M	*USH2A*	AR	p.(Pro5078Arg)	Hetero	p.(GIy2752Arg)	Hetero
OPH-908	40	M	*EYS*	AR	p.(Ser1653fs)	Homo	—	—
OPH-458	29	F	*RP1*	AD	p.(Arg872fs)	Hetero	—	—
OPH-698	53	F	*EYS*	AR	p.(Ser1653fs)	Homo	—	—
OPH-16	44	M	*USH2A*	AR	p.(Gly268Arg)	Homo	—	—
OPH-182	23	F	*RP1*	AR	p.(Cys1399fs)	Homo	p.(Ser2118Asn)	Homo
OPH-980	53	M	*EYS*	AR	p.(Ser1653fs)	Homo	—	—
OPH-613	47	M	*EYS*	AR	p.(Tyr2935*)	Homo	—	—
OPH-159	58	M	*RP1*	AD	p.(Arg872fs)	Hetero	—	—

et al.[21]) using MATLAB software (The MathWorks, Inc., Natick, MA, USA). We marked 12 points on the Bruch's membrane line beginning from the fovea (yellow triangles in Fig. 1A in Komori et al.[21]). The marks were separated by 760 µm in the OCT images. Using cubic spline interpolation, the approximate curvature of the marked points was calculated by the software (yellow and red lines in Fig. 1B in Komori et al.[21]). The curvatures in the 6-mm range including the fovea were selected from the calculated curve. To reduce the effects of the optic nerve head, curvature values outside this range were not used. Using all measured values for the local curvature in 1-µm steps, the mean curvature between ±3 mm from the central fovea (red line in Fig. 1B in Komori et al.[21]) was calculated. Plus values of MMCI indicated a convex shape and minus values indicated a concave shape.

Genetic Diagnosis

Blood samples were collected for the genetic analyses. Genetic diagnosis was performed as described in detail.[6,24,25] A summary of the genetic diagnosis of the RP cases is presented in Table 1.

Table 1. Continued

ID	Age, y	Gender	Causative Genes	Genetic Inheritance Form	Variant 1	Zygosity 1	Variant 2	Zygosity 2
OPH-767	51	M	*EYS*	AR	p.(Cys211Tyr)	Homo	p.(Leu2938Met)	Hetero
OPH-43	52	F	*USH2A*	AR	p.(Pro560Ala)	Homo	p.(Gly2752Arg)	Homo
OPH-552	46	F	*EYS*	AR	p.(Gln3101fs)	Homo	—	—
OPH-129	68	M	*RP1L1*	AR	p.(Ala1009fs)	Homo	—	—
OPH-824	53	F	*EYS*	AR	p.(Tyr2935*)	Homo	—	—
OPH-864	50	F	*EYS*	AR	p.(Tyr2935*)	Homo	—	—
OPH-459	36	F	*USH2A*	AR	p.(Tyr3701*)	Hetero	p.(Ile3620Thr)	Hetero
OPH-465	66	M	*RP1L1*	AR	p.(Arg658*)	Homo	—	—
OPH-293	59	F	*EYS*	AR	p.(Ser1653fs)	Hetero	p.(Met12Thr)	Hetero
OPH-279	50	F	*EYS*	AR	p.(Ser1653fs)	Homo	—	—
OPH-327	52	M	*RP1L1*	AR	p.(Arg658*)	Homo	—	—
OPH-791	42	M	*RP1*	AD	p.(GIn689*)	Hetero	—	—
OPH-222	78	M	*RP1*	AD	p.(Arg872fs)	Hetero	—	—
OPH-617	50	F	*EYS*	AR	p.(Ser1653fs)	Homo	—	—
OPH-51	43	F	*EYS*	AR	p.(Tyr2935*)	Hetero	p.(Ser69fs)	Hetero

The noncanonical splice site variant (c.28+5G>A) in *RPGR* was detected in OPH-783. NA0209 & NA1209 and NA0048 & NA1048 were siblings. AD, autosomal dominant; AR, autosomal recessive; Hetero, heterozygous; Hemi, hemizygous; Homo, homozygous; XL, X-linked.

Statistical Analyses

We determined the significance of the differences in the age, BCVA, AL, EZ width, and MMCI for the five causative genes by Kruskal-Wallis tests. We also compared the MMCIs of each variant for each gene by Kruskal-Wallis tests. We used multiple linear regression analyses to determine the independence of the causative genes contributing to the MMCIs. To adjust for the clinical factors, we included the sex (male or female), age (years, continuous), EZ width (µm, continuous), and AL (mm, continuous) as covariates in the analysis. The MMCIs of the *EYS* eyes were defined as the reference value because the *EYS* is the most common causative gene of RP in the Japanese population,[26,27] and the distribution of MMCI values in *EYS* eyes was similar to that of all the RP cases in our previous study (Table 2).[21] We quantified the effects of the other genes relative to that of the *EYS* value. The MMCI values were converted to absolute square numbers to treat them as normal distributions. We considered a P value of <0.05 to be statistically significant. The R software version 3.4.4 was used for all statistical analyses (available in the public domain at http://www.R-project.org/).

Results

Clinical and Genetic Characteristics of Patients With RP

The median BCVA of all the patients with RP was 0.30 logMAR units, and the median AL of all the patients with RP was 24.0 mm. In all of the eyes, the EZ was fully or partially disrupted. The median MMCI for all RP eyes was -12.6×10^{-5} µm^{-1}.

The clinical and genetic characteristics of the patients with RP for each causative gene are presented in Table 1 and Table 2. There were 31 cases with the *EYS* variants (10 men and 21 women), 11 cases with *USH2A* variants (6 men and 5 women), 6 cases with *RPGR* variants (6 men), 13 cases with *RP1* variants (6 men and 7 women), and 4 cases with *RP1L1* variants (3 men and 1 woman). Of the 13 *RP1*-related patients with RP, there were eight ARRP cases, and seven of them had an Alu insertion in the *RP1* gene, which has been reported as a frequent causative variant of patients with *RP1*-related RP in Japan.[25] The common variant in *EYS* [p.(Ser1653fs)] was detected in 16 cases, and none of these patents were relatives.[26,27] No significant differences were observed in the AL, BCVA, or the EZ width among the different causative genes (Table 2). However, we found significant differences in the age and MMCI among the different causative genes ($P = 0.01$ and $P = 0.02$, respectively).

Representative Fundus Photographs and SD-OCT Images of Patients With RP for Each Causative Gene

The fundus photographs and horizontally scanned SD-OCT images of six right eyes of representative patients with RP with different causative genes (cases 1–6) are shown

Table 2. Characteristics of RP Cases Among Causative Genes

Parameter	*EYS* Eyes ($n = 31$)	*USH2A* Eyes ($n = 11$)	*RPGR* Eyes ($n = 6$)	*RP1* Eyes ($n = 13$)	*RP1L1* Eyes ($n = 4$)	*P* Value
Age, y	50.16 ± 10.00	48.28 ± 9.86	43.18 ± 15.95	38.18 ± 19.43	63.51 ± 7.44	0.01*
AL, mm	24.18 ± 1.00	24.34 ± 1.14	24.85 ± 1.82	23.46 ± 1.47	23.84 ± 1.00	0.19
BCVA, logMAR	0.38 ± 0.56	0.25 ± 0.31	0.71 ± 0.71	0.79 ± 0.81	0.56 ± 0.78	0.34
EZ width, µm	1465.7 ± 1419.7	1393.00 ± 965.61	1090.8 ± 1305.02	1244.00 ± 1797.80	2234.00 ± 2410.23	0.68
MMCI, $\times 10^{-5}$, µm^{-1}	−15.54 ± 13.63	−10.35 ± 3.92	−35.81 ± 11.73	−14.71 ± 10.76	−13.84 ± 6.39	0.02*

Values are presented as mean ± SD (standard deviation).
*Statistical significance by Kruskal-Wallis test.

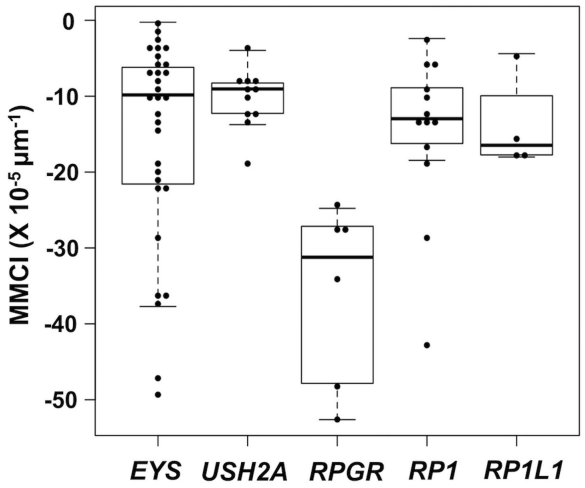

Figure 2. Distribution of MMCIs of RP eyes among causative genes, *EYS*, *USH2A*, *RPGR*, *RP1*, and *RP1L1* is shown. The box length represents the interquartile range, and the middle line depicts the median. MMCI, the mean macular curvature index; RP, retinitis pigmentosa.

in Figure 1. In the *EYS* eyes, one case had a flat macula (Fig. 1A) and another case had a steep macula (Fig. 1B). The *USH2A* (Fig. 1C), *RP1* (Fig. 1E), and *RP1L1* eyes (Fig. 1F) had relatively flat maculae. In contrast, the *RPGR* eye had a steep macula (Fig. 1D).

Distribution of MMCIs of RP Eyes Among Causative Genes

The distribution of the MMCIs of the RP eyes among the causative genes is shown in Figure 2. The MMCIs ranged from -52.62×10^{-5} µm^{-1} to -0.26×10^{-5} µm^{-1}. Interestingly, the MMCI of all *RPGR*-related RP cases was less than -24×10^{-5} µm^{-1}, indicating that the *RPGR* eyes had the steepest curvature. In contrast, all of the MMCIs of the *USH2A* eyes and *RP1L1* eyes were greater than -20×10^{-5} µm^{-1}, indicating that these eyes had a flatter macular curvature. In addition, we observed a wide range of MMCIs in the *EYS* and *RP1* eyes (Table 2 and Fig. 2). The median MMCI was -31.2×10^{-5}/µm for the *RPGR* eyes, -16.5×10^{-5}/µm for the *RP1L1* eyes, -13.0×10^{-5}/µm for the *RP1* eyes, -9.8×10^{-5}/µm for the *EYS* eyes, and -9.0×10^{-5}/µm for the *USH2A* eyes. The *RPGR* eyes had the steepest curvatures and were significantly steeper than that of the *RP1L1* ($P = 0.01$), *RP1* ($P = 0.003$), *USH2A* ($P = 0.0002$), and *EYS* ($P = 0.003$) eyes.

Correlations Between MMCI and Clinical Parameters

The significance of the correlations between age, BCVA, AL, and EZ width and the MMCI was determined for all RP eyes. The MMCI was significantly correlated with the AL and the EZ width ($P = 0.03$ and $P = 0.02$, respectively), although the correlation coefficients were relatively low. On the other hand, the MMCI was not correlated with age or the BCVA ($P = 0.87$ and $P = 0.63$, respectively). The significant correlation observed between MMCI and AL was consistent with the results of our previous study.[21]

Table 3. Results of Multiple Linear Regression Analysis for Independence of Causative Genes Contributing to MMCIs

	RP Cases ($n = 65$)		
Gene	**Estimate**	**Standard Error**	***P* Value**
USH2A	3.92×10^{-5}	3.47×10^{-5}	0.26
RPGR	-2.42×10^{-4}	4.80×10^{-5}	5.30×10^{-6}
RP1	-2.50×10^{-5}	3.60×10^{-5}	0.49
RP1L1	5.57×10^{-6}	5.50×10^{-5}	0.92

Results of multiple linear regression analysis for independence of causative genes contributing to the MMCIs. To adjust for the clinical factors, we included the sex (male or female), age (years, continuous), EZ width (µm, continuous), and AL (mm, continuous) as covariates in the analysis. The effect of the *EYS* gene on MMCI was defined as a reference. We quantified the effects of other genes. The MMCI values were converted to absolute square numbers to treat them as normal distributions.

Multiple Linear Regression Analysis for Independence of Causative Genes Contributing to MMCIs

Multiple linear regression analyses were performed to assess the independence of the causative genes contributing to the MMCIs after adjustment for age, sex, AL, and EZ width (Table 3). We used the effect of the *EYS* on MMCI as a reference and quantified the effects of the other genes relative to that of *EYS*. The MMCI values were converted to absolute square numbers to treat them as being normally distributed. Compared with the effect of *EYS* as the reference gene, *RPGR* significantly affected the MMCI values ($P = 5.30 \times 10^{-6}$). On the other hand, the effects of the other genes, *USH2A*, *RP1,* and *RP1L1*, were not significantly affected compared with the *EYS* gene ($P = 0.26$, $P = 0.49$, and $P = 0.92$, respectively).

Variant-Based Analyses

We compared the MMCIs of each homozygous variant of each AR gene, including p.(Ser1653fs), p.(Tyr2935*), p.(Gly2186Glu), p.(Cys211Tyr), and p.(Gln3101fs) in *EYS*; p.(Cys934Trp), p.(Gly268Arg), and p.(Pro560Ala) in *USH2A*; and p.(Arg658*) and p.(Ala1009fs) in *RP1L1* (Table 1). For *RPGR*, we compared the MMCIs of each hemizygous variant [p.(Glu746fs), p.(Glu802fs), p.(Thr575fs), p.(Gly718fs)] and one splice-site variant (c.28+5G>A) (Table 1). We also compared the MMCIs of homozygous variants of *RP1*-related ARRP [p.(Tyr1352Alafs*9) and p.(Cys1399fs)] or heterozygous variants of *RP1*-related ADRP [p.(Glu661*), p.(Arg872fs), and p.(Gln689*)], because the inheritance pattern of this gene can be autosomal recessive or autosomal dominant (Table 1). Significant differences in the MMCIs of each variant were not observed for each gene (Kruskal-Wallis tests). We further examined the MMCI of *EYS*-related RP cases with the most frequent homozygous variants [p.(Ser1653fs) in *EYS*] and observed that MMCI varied even within the same variants (Supplementary Fig. S1).

Discussion

Our findings showed that the steepness of macular curvature in RP eyes differs among the different causative genes for RP. More specifically, the eyes with the *RPGR* gene had the steepest curvature compared to the other ciliopathy-related

genes. Earlier studies have reported the findings in *RPGR* eyes complicated by high myopia[28–31] and on the relationship between *RPGR*-related RP and pathologic myopia.[31,32] However, the macular curvature in these eyes was not mentioned. Our study showed that the macular curvature in eyes with *RPGR*-related RP was steeper than that in eyes with RP caused by other genes, and the effects of *RPGR* on MMCI were significant even after adjusting for AL. These findings indicate that the *RPGR* gene affected the macular curvature independently. Considering that *RPGR*-related X-linked RP is the target of current clinical trials of adeno-associated viral-mediated gene replacement therapy,[11,33,34] the MMCI may be a useful parameter to evaluate the characteristics of this macula structure in the preoperative evaluations for the prevention of complications of subretinal injection, such as a macular hole. An observation of the MMCI before injection into the subretinal space could provide information on the appropriate angle, site, and injection dose in clinical trials.

We also found that the distribution of the MMCIs differed among the causative genes, although the MMCI of RP caused by each gene was lower than that of controls ($-6.63 \pm 5.63 \times 10^{-5}$ μm^{-1}).[21] The *EYS* eyes had a wide range of MMCI, and in contrast, the *USH2A* and *RP1L1* eyes had a flat macula and a narrow range of distribution of the MMCI. We could differentiate the effects on the specific phenotype of RP among causative genes using the MMCI.

Our results also indicated that there are morphologic differences among the ciliopathy-related genes. Although most of the genes examined, *USH2A*, *RPGR*, *RP1*, and *RP1L1*, encode proteins located in the photoreceptor cilia,[7–12] earlier studies have reported differences in the location of the encoded protein in the photoreceptors.[10] Interestingly, the protein of *RPGR* is located only in the basal body of the cilium.[10] Thus, we hypothesize that the abnormalities of the basal body of the cilia might lead to structural changes and steep macular curvature. However, the mechanisms that lead to this difference in MMCI among genes need additional experimental data.

In a previous study, Khan et al.[18] reported their findings in cases of recessive early-onset retinal dystrophy with macular staphyloma caused by the *C21orf2* gene, which encodes a protein that is localized to the photoreceptor primary cilium. However, reports on macular curvature in inherited retinal dystrophy, including RP, and detailed evaluations of the relationship between macular curvature and visual function are limited. Therefore, an investigation of the relationship between increased macular curvature and the vitreous body, vascular abnormalities, choroid, and the central visual function is necessary. The results of this study showed the steepest curvature in *RPGR*-related RP, which was previously described to have a severe course.[1,28] This suggests that MMCI is somehow related to disease severity. If the steep curvature led to RP progression, the reduction of macular curvature might be a potential target for treatment. Increasing the number of cases, including cases with other causative genes, will also be important in future studies.

This study has several strengths. We collected a relatively large number of cases with genetically identified causative genes and quantified the macular curvature for each causative gene. In addition, we verified the effects of the genes on the MMCI after adjusting for other parameters.

There are also limitations in this study. This was a cross-sectional and retrospective analysis with potential selection biases. RP is a rare disease, and the number of genetically solved cases is limited. The *RPGR*-related RP is known to have a severe course, and it is assumed that the EZ line was shorter at a younger age. However, the number of subjects with RP caused by each gene in this study was small, and it is difficult to evaluate the clear trends by age and EZ line for each gene. In variant-based analysis, we could not detect significant differences in the phenotype-genotype correlation because most of the cases consisted of only one patient if we divided groups by each variant. There were several cases with the most frequent homozygous variant [p.(Ser1653fs) in *EYS*], and our results suggest that the MMCIs also varied among cases caused by the same causative variant. However, further comparisons with other variants were difficult; therefore, the small size of our sample was a limitation for variant-based statistical evaluations. In addition, most of the *RPGR*-related RP cases were caused by frameshift variants except for one case (OPH-783). Previous reports have suggested that frameshift variants of the *RPGR* cause more severe clinical alterations; therefore, this may have limited our results (Table 1). Further multicenter studies are needed to collect cases to reduce the selection bias.

In conclusion, our results suggest that the steepness of the macular curvature is significantly associated with the causative genes for RP. The *RPGR* gene had a stronger effect on the steep macular curvature than the other ciliopathy-related genes.

Acknowledgments

The authors thank Duco Hamasaki (Bascom Palmer Eye Institute) for the discussions and editing the final version of the manuscript, as well as Yukihide Momozawa and the members of the Laboratory for Genotyping Development, RIKEN Center for Integrative Medical Sciences.

Supported by the Japan Society for the Promotion of Science (JSPS) KAKENHI (grant 19K09928 to SU) and Takayanagi Retina Research Award (to SU).

Disclosure: **Y. Koyanagi**, None; **S. Ueno**, Novartis Pharma K.K. (F), Tomey Corporation (F), Nidek Company (F), Canon Life Care Solutions (F), HOYA Company (F); **Y. Ito**, Alcon Japan (F), Bayer Health Care (F), Canon Life Care Solutions (F), Carl Zeiss Meditec (F), Kowa Pharmaceutical (F), Novartis Pharma K.K. (F), Pfizer Japan (F), Santen Pharmaceutical (F); **T. Kominami**, None; **S. Komori**, None; **M. Akiyama**, Nidek Company (F); **Y. Murakami**, None; **Y. Ikeda**, Nidek Company (F), HOYA Corporation (F, C), Otsuka Pharmaceutical (F), Santen Pharmaceutical (F), Novartis Pharma K.K. (F), Senju Pharmaceutical (F), Kowa Pharmaceutical (F), Bayer Health Care (F); **K.-H. Sonoda**, None; **H. Terasaki**, Nidek Company (F), Rohto Pharmaceutical (F), Otsuka Pharmaceutical (F), Pfizer Japan (F), Santen Pharmaceutical (F), Alcon Japan (F), Novartis Pharma K.K. (F), Carl Zeiss Meditec (F, C), Senju Pharmaceutical (F), Kowa Pharmaceutical (F), Bayer Health Care (F, C), Wakamoto (F), HOYA Corporation (F), Astellas Pharma (F), Ono Pharmaceutical (C), Sanwa Kagaku Kenkyusho (F), Aichi Ophthalmologists Association (F), Nitten Pharmaceutical (F), Takeda Pharmaceutical Company (F), Chiba Ophthalmologist Association (F), Japan Medical Association (F), Fukushima Ophthalmologist Association (F)

References

1. Verbakel SK, van Huet RAC, Boon CJF, et al. Non-syndromic retinitis pigmentosa. *Prog Retin Eye Res*. 2018;66:157–186.
2. Hartong DT, Berson EL, Dryja TP. Retinitis pigmentosa. *Lancet*. 2006;368:1795–1809.
3. Campochiaro PA, Mir TA. The mechanism of cone cell death in retinitis pigmentosa. *Prog Retin Eye Res*. 2018;62:24–37.

4. Oishi M, Oishi A, Gotoh N, et al. Comprehensive molecular diagnosis of a large cohort of Japanese retinitis pigmentosa and Usher syndrome patients by next-generation sequencing. *Invest Ophthalmol Vis Sci*. 2014;55:7369–7375.
5. Maeda A, Yoshida A, Kawai K, et al. Development of a molecular diagnostic test for retinitis pigmentosa in the Japanese population. *Jpn J Ophthalmol*. 2018;62:451–457.
6. Koyanagi Y, Akiyama M, Nishiguchi KM, et al. Genetic characteristics of retinitis pigmentosa in 1204 Japanese patients. *J Med Genet*. 2019;56:662–670.
7. Adams NA, Awadein A, Toma HS. The retinal ciliopathies. *Ophthalmic Genet*. 2007;28:113–125.
8. Liu Q, Zhang Q, Pierce EA. Photoreceptor sensory cilia and inherited retinal degeneration. *Adv Exp Med Biol*. 2010;664:223–232.
9. Hildebrandt F, Benzing T, Katsanis N. Ciliopathies. *N Engl J Med*. 2011;364:1533–1543.
10. Estrada-Cuzcano A, Roepman R, Cremers FP, den Hollander AI, Mans DA. Non-syndromic retinal ciliopathies: translating gene discovery into therapy. *Hum Mol Genet*. 2012;21:R111–R124.
11. Dias MF, Joo K, Kemp JA, et al. Molecular genetics and emerging therapies for retinitis pigmentosa: basic research and clinical perspectives. *Prog Retin Eye Res*. 2018;63:107–131.
12. Takahashi VKL, Xu CL, Takiuti JT, et al. Comparison of structural progression between ciliopathy and non-ciliopathy associated with autosomal recessive retinitis pigmentosa. *Orphanet J Rare Dis*. 2019;14:187.
13. Alfano G, Kruczek PM, Shah AZ, et al. EYS is a protein associated with the ciliary axoneme in rods and cones. *PLoS One*. 2016;11:e0166397.
14. Lu Z, Hu X, Liu F, et al. Ablation of EYS in zebrafish causes mislocalisation of outer segment proteins, F-actin disruption and cone-rod dystrophy. *Sci Rep*. 2017;7:46098.
15. Xu X, Fang Y, Yokoi T, et al. Posterior staphylomas in eyes with retinitis pigmentosa without high myopia. *Retina*. 2019;39:1299–1304.
16. Kuniyoshi K, Sakuramoto H, Yoshitake K, et al. Longitudinal clinical course of three Japanese patients with Leber congenital amaurosis/early-onset retinal dystrophy with RDH12 mutation. *Doc Ophthalmol*. 2014;128:219–228.
17. Toma C, Ruberto G, Marzi F, et al. Macular staphyloma in patients affected by Joubert syndrome with retinal dystrophy: a new finding detected by SD-OCT. *Doc Ophthalmol*. 2018;137:25–36.
18. Khan AO, Eisenberger T, Nagel-Wolfrum K, Wolfrum U, Bolz HJ. C21orf2 is mutated in recessive early-onset retinal dystrophy with macular staphyloma and encodes a protein that localises to the photoreceptor primary cilium. *Br J Ophthalmol*. 2015;99:1725–1731.
19. Parmeggiani F, De Nadai K, Piovan A, Binotto A, Zamengo S, Chizzolini M. Optical coherence tomography imaging in the management of the Argus II retinal prosthesis system. *Eur J Ophthalmol*. 2017;27:e16–e21.
20. Smirnov VM, Marks C, Drumare I, Defoort-Dhellemmes S, Dhaenens CM. Severe retinitis pigmentosa with posterior staphyloma in a family with c.886C>A p.(Lys296Glu) RHO mutation. *Ophthalmic Genet*. 2019;40:365–368.
21. Komori S, Ueno S, Ito Y, et al. Steeper macular curvature in eyes with non-highly myopic retinitis pigmentosa. *Invest Ophthalmol Vis Sci*. 2019;60:3135–3141.
22. Kaplan J, Bonneau D, Frezal J, Munnich A, Dufier JL. Clinical and genetic heterogeneity in retinitis pigmentosa. *Hum Genet*. 1990;85:635–642.
23. Kominami T, Ueno S, Kominami A, et al. Associations between outer retinal structures and focal macular electroretinograms in patients with retinitis pigmentosa. *Invest Ophthalmol Vis Sci*. 2017;58:5122–5128.
24. Kominami A, Ueno S, Kominami T, et al. Case of cone dystrophy with normal fundus appearance associated with biallelic POC1B variants. *Ophthalmic Genet*. 2018;39:255–262.
25. Nikopoulos K, Cisarova K, Quinodoz M, et al. A frequent variant in the Japanese population determines quasi-Mendelian inheritance of rare retinal ciliopathy. *Nat Commun*. 2019;10:2884.
26. Hosono K, Ishigami C, Takahashi M, et al. Two novel mutations in the EYS gene are possible major causes of autosomal recessive retinitis pigmentosa in the Japanese population. *PLoS One*. 2012;7:e31036.
27. Iwanami M, Oshikawa M, Nishida T, Nakadomari S, Kato S. High prevalence of mutations in the EYS gene in Japanese patients with autosomal recessive retinitis pigmentosa. *Invest Ophthalmol Vis Sci*. 2012;53:1033–1040.
28. Tee JJ, Smith AJ, Hardcastle AJ, Michaelides M. RPGR-associated retinopathy: clinical features, molecular genetics, animal models and therapeutic options. *Br J Ophthalmol*. 2016;100:1022–1027.
29. Tee JJL, Yang Y, Kalitzeos A, Webster A, Bainbridge J, Michaelides M. Natural history study of retinal structure, progression, and symmetry using ellipzoid zone metrics in RPGR-associated retinopathy. *Am J Ophthalmol*. 2019;198:111–123.
30. Mawatari G, Fujinami K, Liu X, et al. Clinical and genetic characteristics of 14 patients from 13 Japanese families with RPGR-associated retinal disorder: report of eight novel variants. *Hum Genome Var*. 2019;6:34.
31. Parmeggiani F, Barbaro V, De Nadai K, et al. Identification of novel X-linked gain-of-function RPGR-ORF15 mutation in Italian family with retinitis pigmentosa and pathologic myopia. *Sci Rep*. 2016;6:39179.
32. Sanchez Tocino H, Diez Montero C, Villanueva Gomez A, Lobo Valentin R, Montero-Moreno JA. Phenotypic high myopia in X-linked retinitis pigmentosa secondary to a novel mutation in the RPGR gene. *Ophthalmic Genet*. 2019;40:170–176.
33. Cehajic Kapetanovic J, McClements ME, Martinez-Fernandez de la Camara C, MacLaren RE. Molecular strategies for RPGR gene therapy. *Genes (Basel)*. 2019;10:674.
34. Cehajic-Kapetanovic J, Xue K, Martinez-Fernandez de la Camara C, et al. Initial results from a first-in-human gene therapy trial on X-linked retinitis pigmentosa caused by mutations in RPGR. *Nat Med*. 2020;26:354–359.

Investigative Ophthalmology & Visual Science